Nano Energy 54 (2018) 59–65

Contents lists available at ScienceDirect

Nano Energy

journal homepage: www.elsevier.com/locate/nanoen

Full paper

Activate metallic copper as high-capacity cathode for lithium-ion batteries via nanocomposite technology

Ying Huang[a,b,1], Wang Zhang[d,1], Sibai Li[c,1], Wei Luo[a,*], Zhimei Huang[d], Chun Fang[d], Mouyi Weng[c], Jiaxin Zheng[c], Feng Pan[c,*], Qingju Liu[b,*], Yunhui Huang[a,d,**]

[a] Institute of New Energy for Vehicles, School of Materials Science and Engineering, Tongji University, Shanghai 201804, PR China
[b] School of Materials Science and Engineering, Yunnan Key Laboratory for Micro/Nano Materials and Technology, Yunnan University, Kunming 650091, PR China
[c] School of Advanced Materials, Shenzhen Graduate School, Peking University, Shenzhen 518055, PR China
[d] State Key Laboratory of Material Processing and Die & Mould Technology, School of Materials Science and Engineering, Huazhong University of Science and Technology, Wuhan 430074, PR China

ARTICLE INFO

Keywords:
Lithium-ion batteries
Cathode
Electrospinning
Nanofiber
Metallic Cu

ABSTRACT

In this work, metallic copper serving as a high-performance cathode in lithium-ion based carbonate electrolyte has been demonstrated. Computational modelling and in-situ ultraviolet-visible spectra confirm that Cu cathode experiences a two-electrons redox reaction: $Cu \leftrightarrow Cu^{2+} + 2e^-$ during charge/discharge process. By using one-dimensional (1D) nano-structure design and surface modification strategy, the Cu cathode delivers a reversible capacity of 635 mAh/g_{Cu} with a high output voltage of 3.61 V and affords a superior rate capability. With $Li_4Ti_5O_{12}$ as anode, a $Cu/Li_4Ti_5O_{12}$ full cell exhibits a discharge capacity of 601 mAh/g_{Cu} and an energy density of 1202 Wh/kg_{Cu}. The strategy of using metallic Cu as cathode in lithium-ion batteries is quite simple and broadly applicable, which may provide new opportunities for many other non-aqueous rechargeable batteries.

1. Introduction

Lithium-ion batteries (LIBs) are currently indispensable power supply for portable electronic devices due to their high energy density and good cyclability, which have generated great impacts on the human society [1]. To meet the ever-growing demand, increasing energy density and power density of LIBs has become research focus in battery community for decades [1–6]. The energy density of LIBs fundamentally depends on specific capacity of electrode materials and cell output voltage. Traditional electrode materials including layered metal oxides [7–11], polyanionic compounds [12–15], and layered graphite anodes [16–18] have limited space to accommodate enough Li ions, which deliver relatively low specific capacities due to the intercalation/de-intercalation mechanism. On the other hand, the batteries based on conversion chemistry present much larger capacities, such as lithium-sulfur (Li-S) and lithium-oxygen (Li-O_2) batteries [19,20]. Since these systems meet many critical challenges especially poor cyclability, recent studies have shown that the batteries with conversion-type cathodes may be a good solution to reach 500 Wh/kg and offer comparable driving range for electric vehicles to conventional vehicles with internal combustion engine [21,22].

Metallic copper (Cu) has evolved to fill many critical roles in industry and our daily life due to its abundance and high thermal/electrical conductivity. As we know, Cu can serve as a positive electrode in Daniell cell. The voltage of the cell is about 1.1 V in aqueous electrolyte by simply subtracting the potential of Zn^{2+}/Zn redox couple (−0.76 V *vs.* SHE) from that of Cu^{2+}/Cu redox couple (+0.34 V *vs.* SHE) [23]. In non-aqueous LIBs, Cu usually acts as current collector instead of electrode. In fact, the potential gap between Cu^{2+}/Cu and Li^+/Li is as high as 3.38 V according to the standard electrode potential table. Moreover, the theoretical capacity of Cu based on the two-electrons reaction ($Cu \leftrightarrow Cu^{2+} + 2e^-$) reaches 837 mAh/g [24]. Pairing Cu^{2+}/Cu and Li^+/Li electrodes theoretically gives an energy density as high as 2829 Wh/kg_{Cu}, which is almost comparable to Li-S batteries. This leads to a fundamental question: can metallic Cu directly serve as a cathode in non-aqueous battery systems to deliver a high voltage output?

The present challenge of coupling Cu/Li in a single organic electrolyte system lays on dissolution and diffusion of Cu^{2+} ions in electrolyte, which is similar to the well-known shuttle effect in Li-S batteries [25]. Many strategies have been proposed to solve the dissolution

* Corresponding authors.
** Corresponding author at: Institute of New Energy for Vehicles, School of Materials Science and Engineering, Tongji University, Shanghai 201804, PR China.
E-mail addresses: weiluo@tongji.edu.cn (W. Luo), panfeng@pkusz.edu.cn (F. Pan), qjliu@ynu.edu.cn (Q. Liu), huangyh@tongji.edu.cn (Y. Huang).
[1] These authors contributed equally to this work.

https://doi.org/10.1016/j.nanoen.2018.09.064
Received 23 August 2018; Received in revised form 21 September 2018; Accepted 30 September 2018
Available online 02 October 2018

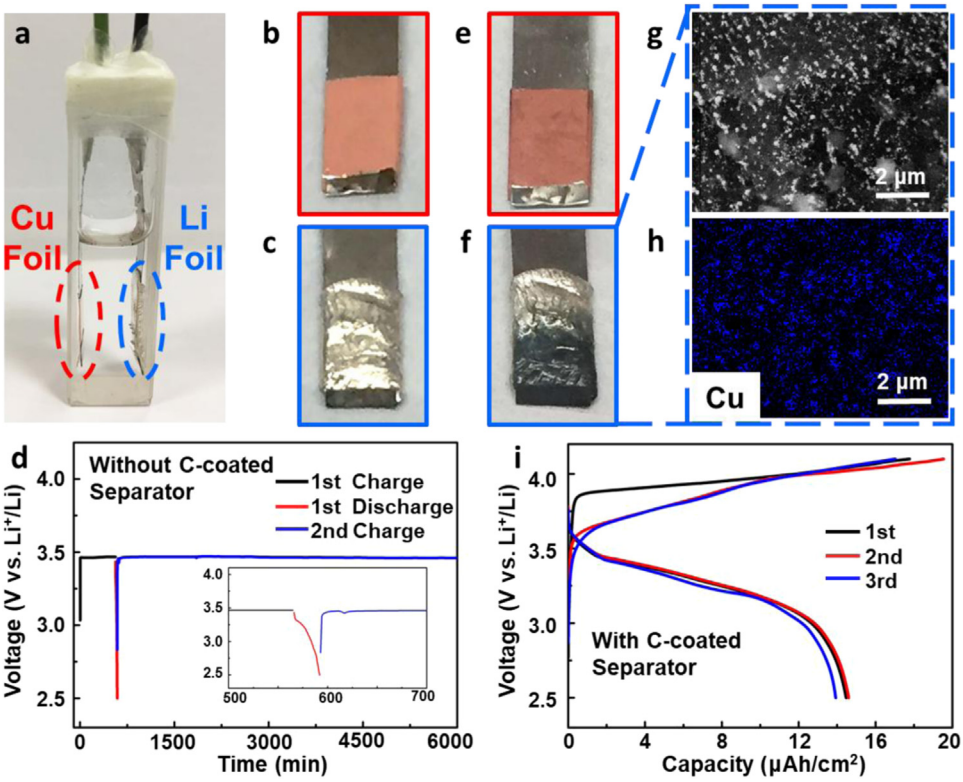

Fig. 1. (a) Optical photographs of the transparent half cell with (b) Cu foil cathode and (c) Li foil anode. (d) Galvanostatic charge/discharge curves of the transparent cell at a current of 0.05 mA g-1. Optical photographs of (e) Cu foil cathode and (f) Li foil anode, (g, h) SEM and corresponding Cu elemental mapping images of Li foil anode after charging for 10 h. (i) Voltage profiles of coin-cell type Cu/Li half cell with a C-coated Celgard separator.

issue of polysulfides in Li-S batteries [26]. Inspired by the great progress of engineering separators in Li-S batteries [27], we demonstrate in this work that metallic Cu cathode can serve as a high-performance cathode in conventional non-aqueous LIBs. Theoretical calculation illustrated that the metallic Cu is oxidized to Cu^{2+} directly during charge process and the discharge process undergoes two steps: Cu^{2+} is first reduced to Cu^{+} and then further reduced back to metallic Cu. By using a nanosized metallic Cu/carbon nanofiber (Cu@CNFs) composite and a carbon-coated separator in the cell configuration [28,29], a high reversible capacity of 635 mAh/g_{Cu} with an average potential of 3.61 V (*vs.* Li^{+}/Li) are obtained in a common carbonate electrolyte. To further improve the cycle stability, a simple surface modification strategy was employed, which enabled the Cu cathode exhibit a superior rate capability and along with a stable cycle performance. With $Li_4Ti_5O_{12}$ (LTO) as anode, the Cu/LTO full cell exhibits a high discharge capacity up to 601 mAh/g_{Cu}.

2. Results and discussion

The proof-of-concept study was demonstrated using a Cu/Li half cell within a home-made transparent device (Fig. 1a). Planar Cu foil (Fig. 1b and Fig. S1) acted as cathode, Li foil (Fig. 1c and Fig. S2) as anode and 1.0 M $LiClO_4$ in ethylene carbonate (EC)/propylene carbonate (PC) (v/v = 1/1) as electrolyte, while no separator was used. Galvanostatic charge started under 0.05 mA. As shown in Fig. 1d, the voltage of the cell increases rapidly and then a long voltage plateau appears at 3.45 V. This charge process corresponds to the oxidation of Cu foil along with dissolution of Cu^{2+} ions into electrolyte [30]. To keep the charge balance, Li^{+} ions in the electrolyte were reduced and deposited as metallic Li on Li foil. However, the charge process seems interminable over charging time. Thus, we manually stopped the charge process after 10 h and switched the current direction. Surprisingly, the cell presented an extremely short discharge process that the voltage sharply dropped to 2.5 V, suggestive of an irreversible process of Cu dissolution. This should be ascribed to that Cu^{2+} ions diffuse to the Li metal side and are then reduced by Li metal. To prove this hypothesis, we disassembled the cell and characterized the Cu and Li foils after the charge process. The surface of Cu turned slightly grey and a great number of pits appeared (Fig. 1e and Fig. S3). On the anode side, Li foil became black (Fig. 1f). Scanning electron microscopy (SEM) and elemental mapping observation show that Li foil was covered by Cu-containing nanoclusters (Fig. 1g, h and Fig. S4). This indicates that Cu^{2+} ions diffused and deposited on Li foil by reacting with Li [31].

To suppress the diffusion of Cu^{2+} ions, we moved the electrodes into a coin cell and a C-coated Celgard polypropylene (PP) separator was employed (Fig. S5) [32]. As seen in Fig. 1i, the Cu/Li coin cell displays normal charge/discharge curves at a current of 0.05 mA. Compared to the transparent cell (Fig. 1d), the reversibility of Cu electrode in coin cell is greatly improved with the first-cycle coulombic efficiency reaching 75%. To verify the effect of C-coated separator, we examined the surface of Li foil after several cycles. The SEM and mapping images both show that there is no elemental Cu observed on the Li foil (Fig. S6). Overall, the above results prove that metallic Cu can be a reversible cathode for non-aqueous LIBs by simply adjusting the battery configuration. In the corresponding cyclic voltammetry (CV) curves (Fig. S7), a broad peak at 3.91 V appears during the initial anodic scan, indicating the oxidation of Cu while two peaks occurs at 3.52 and 3.33 V in the following cathodic scan present the reduction reactions: $Cu^{2+} \rightarrow Cu +$ and $Cu + \rightarrow Cu$.

As shown in Fig. 1i, the specific capacity of the planar Cu foil is low due to the bulk morphology. To maximize the usage of metallic Cu, we designed a novel Cu@C composite cathode, in which active Cu nanoparticles were anchored on a three-dimensional conductive carbon nanofiber (CNFs) network. The detailed synthetic procedures are described in the Supporting information. The X-ray diffraction (XRD) pattern of Cu@CNFs demonstrate that metallic Cu is successfully obtained (Fig. 2a). SEM (Fig. 2b) and transmission electron microscope (TEM) images (Fig. 2c) show that Cu nanoparticles and CNFs have average sizes of 300 and 100 nm, respectively. A high-resolution TEM (HR-TEM) image (right side in Fig. 2c) on the edge of a single Cu nanoparticle displays a set of parallel fringes with d-spacing of 0.208 nm, corresponding to the (111) plane of Cu. Energy-dispersive X-ray

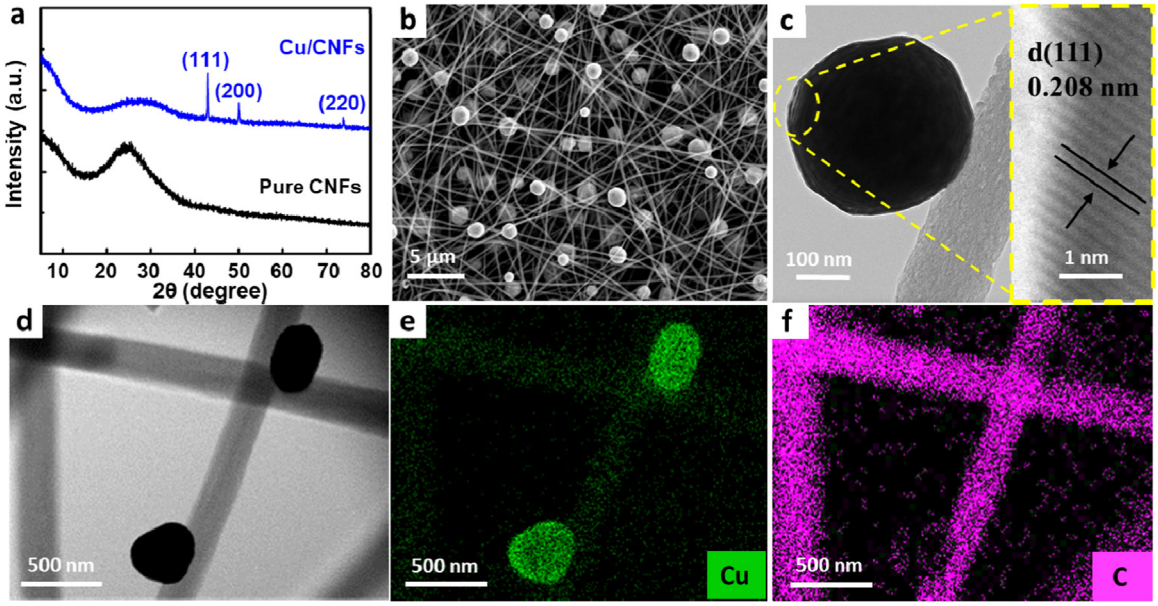

Fig. 2. Phase and morphology characteristics of Cu@CNFs composite. (a) XRD patterns of Cu/CNFs and pure CNF, (b) SEM, (c) TEM and (d-f) element mapping images of Cu@CNFs composite obtained by electrospinning and following thermal reduction.

spectroscopy (EDX) elemental mappings (Fig. 2d-f) show the distribution of Cu and C elements in the composite, demonstrating that Cu nanoparticles are well anchored on the CNFs.

The electrochemical performance of the Cu@CNFs composite was investigated by using the Cu@CNFs composite as cathode, Li foil as anode and C-coated Celgard PP as separator. In Fig. 3a, the Cu@CNFs composite exhibits a relatively flat voltage plateau at 3.61 V. A specific capacity in charge as high as 770 mAh/g is attained, which reaches 91% of the theoretical capacity (837 mAh/g) based on two-electrons reaction. The corresponding discharge process exhibits a specific capacity of

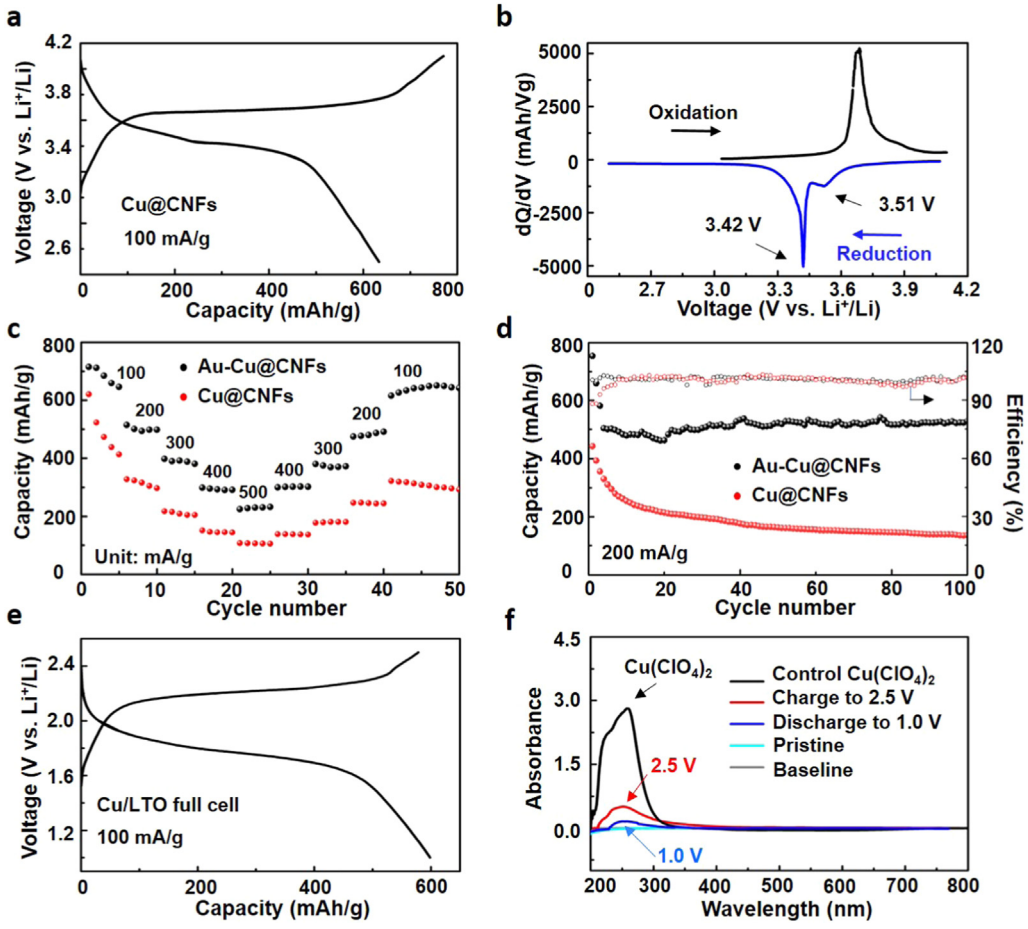

Fig. 3. (a) Voltage profile of Cu@CNFs electrode for the first cycle at 100 mA/g at room temperature. (b) The incremental charge versus potential (dQ/dV) curve of the charge/discharge process for Cu@CNFs electrode. (c) Specific discharge capacities of Cu@CNFs and Au-Cu@CNFs electrodes cycled at various current densities from 100 to 500 mA/g. (d) Cycling performance of Cu@CNFs and Au-Cu@CNFs electrodes at 200 mA/g. (e) Voltage profile of the full cell for the first cycle at 100 mA/g. (f) UV–vis absorption spectra of the electrolyte in the in-situ full cell at different states upon cycling.

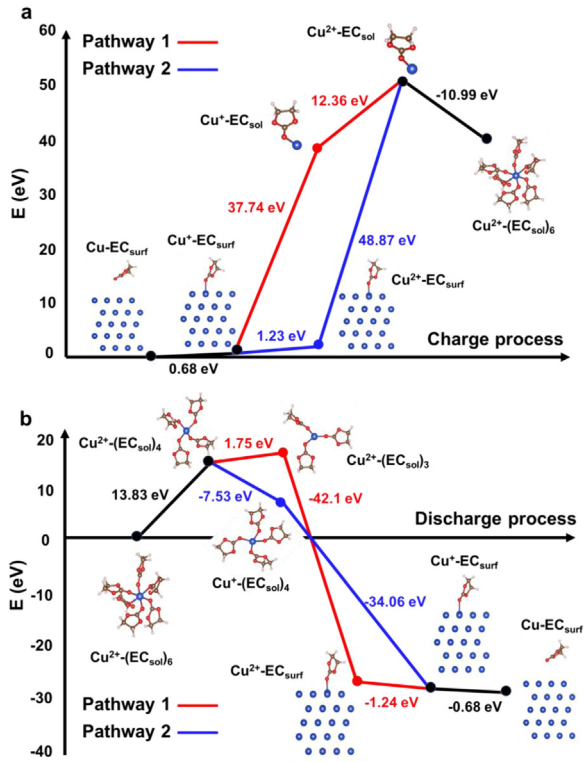

Fig. 4. Theoretical calculation for the redox process of Cu cathode in Cu/Li half cell. Two possible reaction pathways during (a) charge process and (b) discharge process, represented by red and blue lines, respectively. The blue line represents the energy-preferred pathway.

635 mAh/g, indicative of a highly reversible electrochemical redox reaction. Notably, the Cu@CNFs electrode exhibits one charge plateau corresponding to the oxidation process of Cu → Cu^{2+} + $2e^-$. In contrast, a weakly inflection point at 3.42 V divides the discharge curve into two parts. The two reduction steps are clearly evidenced by the incremental charge (dQ) versus potential (dQ/dV) curve (Fig. 3b) that the two cathodic peaks at 3.51 and 3.42 V should be ascribed to Cu^{2+} → Cu^+ and Cu^+ → Cu, respectively.

To understand the electrochemical process, the structure and morphology evolution of Cu@CNFs electrodes were monitored by ex-situ XRD and SEM measurements. In Fig. S8, the XRD peaks of metallic Cu nearly disappear after charging to 4.1 V. It is most likely that Cu was oxidized to Cu^{2+} and dissolved in the electrolyte. After discharge to 2.5 V, the Cu peak at 43°, 50° and 74° are completely restored, confirming that Cu^{2+} was reduced to Cu reversibly. The morphological change of Cu@CNFs composite agrees well with the structure evolution. As shown in Fig. S9, SEM images of Cu@CNFs after charging to 4.1 V display that there are no Cu nanoparticles anchored on the surface of CNFs. Inversely, metallic Cu is redeposited on the surface of CNFs after discharge to 2.5 V (Fig. S10). However, the re-deposited Cu aggregated and formed bulky particles, which is unfavorable to subsequent redox process. We speculate that the aggregation associates with the low surface energy and affinity of Cu^{2+} on CNFs surface [33].

To prevent the aggregation of Cu on CNFs upon repeated cycles, a simple Au nanoparticle coating was applied [34]. SEM images of Au-coated Cu@CNFs (Au-Cu@CNFs) show that Au nanoparticles with diameter from 5 to 20 nm are uniformly covered onto the Cu/CNFs surface (Fig. S11). Interestingly, Au-Cu@CNFs composite exhibits charge capacity of 755 mAh/g and discharge capacity of 751 mAh/g in the first cycle (Fig. S12), indicating an initial coulombic efficiency (CE) as high as 99%. Furthermore, the rate capability of Au-Cu@CNFs is also enhanced compared to Cu@CNFs electrode. As seen in Fig. 3c, the reversible discharge specific capacities of Au-Cu@CNFs are 720, 541, 398, 299 and 225 mAh/g at current densities of 100, 200, 300, 400 and 500 mA/g, respectively. The capacity can be recovered up to 615 mAh/g when the current density turns back to 100 mA/g, suggesting an excellent rate capability. Moreover, Au-Cu@CNFs displays superior long-term stability with a specific capacity of 523 mAh/g at 200 mA/g over 100 cycles (Fig. 3d). To verify the role of Au modification, the morphology of Au-Cu@CNFs composite during redox process were investigated by SEM (Fig. S13) and TEM (Fig. S14). The morphology of Au-Cu@CNFs shows that Cu nanoparticles disappear while Au nanoparticles still adheres on the surface of CNFs after charging to 4.1 V and the redeposited Cu nanoparticles have no aggregation. The morphology change validates that Au modification provides more nucleation sites, and hence promotes the uniform deposition of Cu.

A full cell composed of Au-Cu@CNFs composite cathode and $Li_4Ti_5O_{12}$ (LTO) anode was further fabricated. The charge process of the full cell corresponds to the oxidation from Cu to Cu^{2+} in cathode side and the intercalation of Li ions into LTO in anode side (Fig. S15). The SEM images (Fig. S16) and charge/discharge curve (Fig. S17) of LTO anode are given in the Supporting information. The full cell displays an average working voltage of 2.0 V and delivers a discharge specific capacity of 601 mAh/g (Fig. 3e). To investigate the redox mechanism of metallic Cu in full cell, an in-situ transparent cell using Cu@CNFs cathode and LTO anode was assembled and the electrolyte was tested by UV–vis radiation upon electrochemical reactions. Compared to pristine electrolyte, a new peak located at 257 nm appears after charging to 2.5 V. The new peak corresponds to the characteristic peak of Cu $(ClO_4)_2$ (Fig. 3f), which proves the formation of $Cu(ClO_4)_2$ by: Cu + $2LiClO_4$ → $Cu(ClO_4)_2$ + $2Li^+$. After discharging to 1.0 V, the Cu $(ClO_4)_2$ peak almost disappears, suggesting that most of Cu^{2+} ions are reversibly reduced while a small amount of Cu^{2+} ions are maintained in the electrolyte. This result further demonstrates the electrochemical process we proposed in Cu/Li half cells.

To further understand the electrochemical process of non-aqueous Cu/Li cell, we employed computational modelling based on density functional theory (DFT). The detailed calculation procedure is described in Supporting information. For the charge process, the theoretical calculation confirms that Cu atoms can uptake one solvent molecule and form Cu-solvent at Cu (111) surface before oxidation. The as-formed Cu-$EC_{surface}$ (Cu-EC_{surf}) is continuously oxidized with EC absorption, and finally formed Cu^{2+}-$(EC_{sol})_6$ since Cu^{2+}-$(EC_{sol})_6$ is the most stable structure (Fig. S18). For the charge process, there are two possible pathways (Fig. 4a): one is that Cu-EC_{surf} is oxidized to Cu^+-EC_{surf} at Cu (111) surface and diffuses to the electrode/electrolyte interface to complete oxidation and absorption; the other is that Cu-EC_{surf} is directly oxidized to Cu^{2+}-EC_{surf} at Cu (111) surface and then forms Cu^{2+}-$(EC_{sol})_6$ by absorbing more EC molecules. The corresponding energy values are illustrated in Fig. 4a, and the energies of Cu-EC_{surf}, Cu^+-EC_{surf} and Cu^{2+}-EC_{surf} are listed in Table S1. The reaction energy for Cu^+-EC_{surf} → Cu^+-EC_{sol} (pathway 1) is 37.74 eV while that for Cu^+-EC_{surf} → Cu^{2+}-EC_{surf} (pathway 2) is only 1.23 eV. Obviously, the latter pathway is more favorable. Therefore, we believe that Cu is directly oxidized to Cu^{2+} at Cu (111) surface. Similarly, the following reduction reaction in the discharge process has also two possible pathways, as shown in Fig. 4b. According to the calculation, the reaction energy for Cu^{2+}-$(EC_{sol})_4$ → Cu^{2+}-$(ECsol)_3$ (1.75 eV) pathway 1 is much higher than that of Cu^{2+}-$(EC_{sol})_4$ → Cu^+-$(EC_{sol})_4$ (−7.53 eV) pathway 2. Thus, the pathway 2 is preferred. We further calculated the average voltage of Cu redox process in Cu/Li half cell on the basis of the above-discussed pathways. The calculated average voltage is 3.83 V, which is close to the experimental value. Both the experimental measurement and theoretical calculation demonstrate that Cu cathode experiences a two-electrons redox reaction (Cu ↔ Cu^{2+} + $2e^-$) during charge/discharge processes.

3. Conclusion

In summary, we have demonstrated metallic copper as a splendid cathode material for non-aqueous LIBs through a two-electrons conversion reaction. The as-designed Cu@CNFs nanocomposite exhibits a high output voltage of 3.61 V in LIBs system and delivers a high energy density of 2292 Wh/kg_{Cu}. A simple surface modification by Au coating facilitates the nucleation and growth of Cu upon discharge, which hinders the aggregation of Cu particles and improves the rate and cycling capabilities of Cu cathode. We anticipate that the Cu cathode with high output voltage, high capacity and good stability in non-aqueous LIB systems is available for developing next-generation batteries to meet the ever-growing demand of high energy density. Furthermore, since the reversible redox reaction of Cu cathode is independence of the metal ions in electrolyte salt, we believe that Cu cathode can be further extended to other metal-ion battery systems.

4. Experimental section

4.1. Fabrication of the transparent half cell and full cell

The transparent half cell and in-situ full cell were assembled in cuvettes (size: 12.5(W)*12.5(L)*45(H) mm). For the transparent half cell, Cu foil and Li foil were fixed on two titanium (Ti) foils respectively (size: 6(W)*60(L) mm) using as cathode and anode. Cu@CNFs composite was fixed on a Ti foil as cathode and $Li_4Ti_5O_{12}$ slurry was casted onto a Ti foil as anode for the in-situ full cell. 1.0 mol/L $LiClO_4$ EC/PC (v/v = 1:1) electrolyte was used in two cases.

4.2. Synthesis of electrodes and C-coated separators

4.2.1. Cu@CNFs composite

The Cu@CNFs composite was synthesized by electrospinning and subsequent thermal reduction. The electrospinning precursor solution was made by blending 1 g polyacrylonitrile (PAN) and 0.5 g copper acetate monohydrate ($Cu(CH_3COO)_2{\cdot}H_2O$) in 10 mL N, N-Dimethylformamide (DMF). The precursor solution was kept at 80 °C and stirred for 12 h. Then a high-voltage of 17 kV was applied to the solution during the electrospinning process. The collected fibers were stabilized at 280 °C for 3 h in air and further carbonized at 900 °C for 2 h in H_2/Ar (5% H_2) atmosphere, the heating rate for stabilization and carbonization are 5 °C/min. The final product Cu@CNFs composite film was cut into disks with 8 mm diameter and used as electrode directly. Thermogravimetric analysis (TGA) gives the Cu content in Cu@CNF composite, which is about 50 wt% (Fig. S19). The loading for each electrode is 0.5 mg/cm^2.

4.2.2. Au-Cu@CNFs composite

The Au nanoparticles were directly deposited on the Cu@CNFs surface by Precision etching coating instrument (Gatan 682). The coating time is 150 s and the particles size of Au are 5–20 nm.

4.2.3. $Li_4Ti_5O_{12}$ electrode

The $Li_4Ti_5O_{12}$ electrode is consisted of 60 wt% $Li_4Ti_5O_{12}$, 30 wt% Super P and 10 wt% PVDF. All components were mixed and ground with N-methyl-2-pyrrolidinone solvent to prepare the slurry, casted onto a Cu current collector and completely dried before use. The Loading of LTO is about 2 mg/cm^2.

4.2.4. C-coated separator

The C-coated separator is prepared by uniformly casting carbon slurry on Celgard 2301 polypropylene separator and dried before use. The carbon slurry is consisted of 60 wt% Super P, 20 wt% active carbon and 20 wt% PVDF. All components were mixed and ground with N-methyl-2-pyrrolidinone (NMP) solvent to prepare the slurry.

4.3. Material characterizations

The material morphology was investigated by SEM (SIRION200) and TEM (FEI Tecnai G2 F30). Structure of materials were detected by XRD (PANalytical X'pert PRO-DY2198, Holland) measurements. TG (NETZSCH STA449F3) analysis was carried out in air from room-temperature to 800 °C at a heating rate of 10 °C/min. In-situ UV–vis spectrum was detected on a UV-2550 UV–vis spectrophotometer (Shimadzu, Japan).

4.4. Electrochemical measurements

All the cells were assembled in an argon-filled glove box (O_2 and H_2O less than 1 ppm). In coin-cells, the cathode and anode were separated by a carbon coated Celgard separator. 1.0 M $LiClO_4$ dissolved in a mixture of ethylene carbon (EC) and propylene carbonate (PC) (1:1 by volume) was used as the electrolyte for LIBs. Galvanostatic charge-discharge tests were carried out on a Neware Battery Measurement System at various current densities. CV measurements in the voltage range of 2.5–4.1 V *vs.* Li^+/Li with a scanning rate of 0.05 mV/s were carried out on a CHI 760E electrochemical workstation.

Acknowledgements

We are grateful for the financial support by National Key R&D Program of China (No. 2018YFB0905400, 2016YFB0700600), National Natural Science Foundation of China (No. 51632001), and Shenzhen Science and Technology Research Grant (No. JCYJ20150729111733470 and JCYJ20151015162256516).

Appendix A. Supporting information

Supplementary data associated with this article can be found in the online version at doi:10.1016/j.nanoen.2018.09.064

References

[1] P. Albertus, S. Babinec, S. Litzelman, A. Newman, Nat. Energy 3 (2018) 16–21.
[2] J.T. Xu, J.M. Ma, Q.H. Fan, S.J. Guo, S.X. Dou, Adv. Mater. 29 (2017) 1606454.
[3] J. Lu, Z.H. Chen, Z.F. Ma, F. Pan, L.A. Curtiss, K. Amine, Nat. Nanotechnol. 11 (2016) 1031.
[4] Z.P. Song, H.S. Zhou, Energy Environ. Sci. 6 (2013) 2280–2301.
[5] R. Mukherjee, R. Krishnan, T.-M. Lu, N. Koratkar, Nano Energy 1 (2012) 518–533.
[6] J. Xu, S. Dou, H. Liu, L. Dai, Nano Energy 2 (2013) 439–442.
[7] M.S. Whittingham, Chem. Rev. 104 (2004) 4271–4302.
[8] C.L. Zhang, S.H. Yu, Chem. Soc. Rev. 43 (2014) 4423–4448.
[9] C.L. Tan, Z.C. Lai, H. Zhang, Adv. Mater. 29 (2017) 1701392.
[10] H.G. Jung, M.W. Jang, J. Hassoun, Y.K. Sun, B. Scrosati, Nat. Commun. 2 (2011) 516.
[11] Y. Xia, J. Zheng, C. Wang, M. Gu, Nano Energy 49 (2018) 434–452.
[12] C.V. Subban, M. Ati, G. Rousse, A.M. Abakumov, T.G. Van, R. Janot, J.M. Tarascon, J. Am. Chem. Soc. 135 (2013) 3653–3661.
[13] A.H. Yaghoobnejad, G. Kartik, V.M. Melissa, C. Amitava, J. Mater. Chem. A 3 (2015) 7488–7497.
[14] R.G., J.M. Tarascon, ChemInform, 45, 2014.
[15] Q. Zhao, Y. Zhang, Y. Meng, Y. Wang, J. Ou, Y. Guo, D. Xiao, Nano Energy 34 (2017) 408–420.
[16] E. Yoo, J. Kim, E. Hosono, H.S. Zhou, T. Kudo, I. Honma, Nano Lett. 8 (2008) 2277–2282.
[17] V. Aravindan, Y.S. Lee, S. Madhavi, Adv. Energy Mater. 5 (2015) 1402225.
[18] S. Gyujin, R. Jaegeon, K. Seunghee, B.B. Man, C. Sinho, S. Myoungsoo, L. Sang-Young, P. Soojin, Chem. – Asian J. 11 (2016) 1711–1717.
[19] J. Wang, Y. Li, X. Sun, Nano Energy 2 (2013) 443–467.
[20] J.-G. Wang, K. Xie, B. Wei, Nano Energy 15 (2015) 413–444.
[21] R. Schmuch, R. Wagner, G. Hörpel, T. Placke, M. Winter, Nat. Energy 3 (2018) 267–278.
[22] K. Turcheniuk, D. Bondarev, V. Singhal, G. Yushin, Nature 559 (2018) 467.
[23] X. Dong, Y. Wang, Y. Xia, Sci. Rep. 4 (2014) 6916.
[24] Y.G. Wang, H.S. Zhou, Electrochem. Commun. 11 (2009) 1834–1837.
[25] Q. Pang, X. Liang, C.Y. Kwok, L.F. Nazar, Nat. Energy 1 (2016) 16132.
[26] S.-H. Chung, L. Luo, A. Manthiram, ACS Energy Lett. 3 (2018) 568–573.
[27] Y.S. Su, A. Manthiram, Nat. Commun. 3 (2012) 1166.
[28] C. Fang, Y. Huang, L.X. Yuan, Y.J. Liu, W.L. Chen, Y.Y. Huang, K.Y. Chen, J.T. Han, Q.J. Liu, Y.H. Huang, Angew. Chem., Int. Ed. 129 (2017) 6897–6901.

[29] Y. Huang, C. Fang, R. Zeng, Y.J. Liu, W. Zhang, Y.J. Wang, Q.J. Liu, Y.H. Huang, ChemSusChem 10 (2017) 4704–4708.
[30] Y.S. Kim, S.H. Lee, M.Y. Son, Y.M. Jung, H.K. Song, H. Lee, ACS Appl. Mater. Interfaces 6 (2014) 2039–2043.
[31] M. Jo, S. Park, J. Song, K. Kwon, J. Alloy. Compd. 764 (2018) 112–121.
[32] W. Liu, J.B. Jiang, K.R. Yang, Y.Y. Mi, P. Kumaravadivel, Y.R. Zhong, Q. Fan, Z. Weng, Z.S. Wu, J.J. Cha, H.H. Zhou, V.S. Batistaa, G.W. Brudviga, H.L. Wang, Proc. Natl. Acad. Sci. USA 114 (2017) 3578–3583.
[33] L. Lutz, D.A.D. Corte, Y.H. Chen, D. Batuk, L.R. Johnson, A. Abakumov, L. Yate, E. Azaceta, P.G. Bruce, J.M. Tarascon, A. Grimaud, Adv. Energy Mater. 8 (2018) 1701581.
[34] K. Yan, Z.D. Lu, H.W. Lee, F. Xiong, P.C. Hsu, Y.Z. Li, J. Zhao, S. Chu, Y. Cui, Nat. Energy 1 (2016) 16010.

Ying Huang is a Ph.D. candidate in Yunnan University. She is now a visiting Ph.D. candidate in School of Materials Science and Engineering at Tongji University. Her current research focuses on rechargeable lithium and sodium ion batteries.

Wang Zhang received his B.S. degree in Applied Chemistry (2012) and his Ph.D. in Material Science (2017) from Huazhong University of Science and Technology, China. His current research focuses on rechargeable batteries and their electrode materials for energy storage.

Sibai Li received his B.S. degree in Physics from the School of Physics, Peking University (2015) and M.S. degree in Advanced Materials and Mechanics from the School of Advanced Materials, Peking University (2018). His research interests include: computational materials, 2D materials and energy materials (battery materials and solar energy materials).

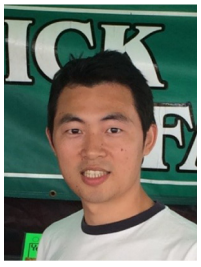

Wei Luo is a Professor in the School of Materials Science and Engineering at Tongji University. He received his Ph.D. from Huazhong University of Science and Technology in 2012. Prior to his current position, Wei worked as a post-doctoral researcher at Oregon State University (2012–2014), and University of Maryland (UMD, 2014–2016) until being promoted to Assistant Research Professor at UMD (2016–2017). His research interests include energy storage and conversion devices, biomass materials, and low-dimensional nanomaterials.

Zhimei Huang received her M.Sc. degree from Huazhong University of Science and Technology (HUST) in 2015. She is now a Ph.D. candidate in HUST. Her current research focuses on the protection of Li metal anode in rechargeable lithium-oxygen battery.

Fang Chun received her Ph.D. from Fudan University in 2008. She then worked as a senior engineer at Evergreen Solar Corp. from 2009 to 2012. After that, she was an R&D manager at Enpower Energy Corp. from 2012 to 2015. Then, she worked as a postdoctoral researcher in Huazhong University of Science and Technology (HUST) from 2015 to 2017. Currently, she is a lecturer in HUST. Her research interests focus on new materials and new devices for energy storage applications.

Mouyi Weng is currently a Ph.D. candidate in Prof. Feng Pan's group at Peking University Shenzhen Graduate School, China. He received his B.S. degree from Tsinghua University in 2015. His research interests include: computational materials, materials simulation algorithms and electronic structure calculation in materials

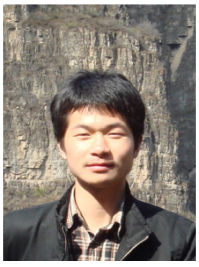

Jiaxin Zheng received his B.S. degree in Physics in 2008 and PhD degree in Condensed Matter Physics in 2013 from Peking University, China. Then he joined the group of Prof. Feng Pan at School of Advanced Materials (SAM), Peking University, Shenzhen Graduate School, China, as a post-doctoral fellow from Oct. 2013 to Oct. 2015. Now he works an associate Professor at SAM. His research interests include: computational materials, energy materials (battery materials, solar energy, thermoelectric materials), nanomaterials, nanoelectronics.

Prof. Feng Pan, National 1000-plan Professor, Founding Dean of School of Advanced Materials , Peking University Shenzhen Graduate School, Director of National Center of Electric Vehicle Power Battery and Materials for International Research, got B.S. from Dept. Chemistry, Peking University in1985 and PhD from Dept. of P&A Chemistry , University of Strathclyde, Glasgow, UK with "Patrick D. Ritchie Prize" for the best Ph.D. in 1994. Prof. Pan has been engaged in fundamental research and product development of novel energy conversion and storage materials & devices. As Chief Scientist, Prof. Pan led 12 entities to win National Key project of Material Genomic Engineering for Solid State Li-ion Battery in China in 2016. He has been selected as one of the 2018 winner of ECS Battery Division Technology Award.

Qingju Liu is a professor at the College of Materials Science and Engineering, Yunnan University. She earned her MS in Electronic-physics and Device from Huazhong University of Science and Technology in 1990, and PhD in Materials Science from Kunming University of Science and Technology in 2003. Her research interests include nanostructured functional materials and materials for new energy.

Yunhui Huang received his Ph.D. from Peking University in 2000. From 2004–2007, he worked with Professor John Goodenough in the University of Texas at Austin. In 2008, he became a chair professor of materials science in Huazhong University of Science and Technology. He is now the director of Institute of New Energy for Vehicles in Tongji University. His research group works on rechargeable batteries for energy storage and their electrode materials.